World Academy of Science, Engineering and Technology
International Journal of Electrical and Information Engineering
Vol:15, No:7, 2021

Performance of BLDC Motor under Kalman Filter Sensorless Drive

Yuri Boiko, Ci Lin, Iluju Kiringa, Tet Yeap

***Abstract*—**The performance of a permanent magnet brushless direct current (BLDC) motor controlled by the Kalman filter based position-sensorless drive is studied in terms of its dependence from the system's parameters variations. The effects of the system's parameters changes on the dynamic behavior of state variables are verified. Simulated is the closed loop control scheme with Kalman filter in the feedback line. Distinguished are two separate data sampling modes in analyzing feedback output from the BLDC motor: (1) equal angular separation and (2) equal time intervals. In case (1), the data are collected via equal intervals $\Delta\theta$ of rotor's angular position θ_i, i.e. keeping $\Delta\theta$ = const. In case (2), the data collection time points t_i are separated by equal sampling time intervals Δt = const. Demonstrated are the effects of the parameters changes on the sensorless control flow, in particular, reduction of the instability torque ripples, switching spikes, and torque load balancing. It is specifically shown that an efficient suppression of commutation induced instability torque ripples is an achievable selection of the sampling rate in the Kalman filter settings above a certain critical value. The computational cost of such suppression is shown to be higher for the motors with lower induction values of the windings.

***Keywords*—**BLDC motor, Kalman filter, sensorless drive, state variables, instability torque ripples reduction, sampling rate.

I. Introduction

THE sensorless drive of BLDC motor had been reported to deliver an efficient control of BLDC motor when employing various versions of Kalman filter [1] for the purpose of phase synchronization in the motor's windings [2]-[10]. Some advanced architectures have been reported to achieve intelligent operation of sensorless drive for BLDC motor. Specifically, in [4] a hybrid fuzzy/PI controller is suggested with improved efficiency. The disturbance observers allowed achieving adaptive velocity estimations for BLDC motor operation [7]. The implementation of the extended Kalman filter rendered the speed and rotor position estimation of BLDC motor [8]. The sliding mode control with Kalman filter for BLDC motor had been verified [9]. Applications of BLDC motor control in the aerospace industry is further pursued [10]. However, the overall picture is still short on covering the dependencies of the sensorless control from internal motor's parameters, outside disturbances and parameters of operating circuits. This void needs to be filled in with further research efforts, in part presented herewith.

Yuri Boiko*, Ci Lin, Iluju Kiringa, and Tet Yeap are with the School of Information Technology and Engineering of the University of Ottawa, Ottawa, ON K1N 6N5, Canada (*corresponding author, e-mail: yboik074@uottawa.ca, clin072@uottawa.ca, iluju.kiringa@uottawa.ca tyeap@uottawa.ca).

II. Problem Formulation

While there are well established cases of operational sustainability of application of Kalman filter based sensorless control to drive BLDC motors, there is still a need of topic exploration for the wider range of relevant motor parameters in order to see the effects of those parameters changes on the performance of the sensorless control schemes. This would allow verifying the limits to be observed, anticipate potential problems in case of external disturbances and/or instabilities as well as possibly to develop counter measures preventing the induced disruptions in motor operation. Therefore, the goal in this article is to verify the operational efficiency of the Kalman filter based sensorless control scheme for a wide range of system's parameters.

III. Methodology

The methodology chosen herewith is simulation and modeling. The BLDC model is relying on known electro-magnetic interactions in the motor's windings in the rotating magnetic field of permanent magnets. The Kalman filter observes the current values in the motor's windings and estimates commutation instants for the windings, sending switching signals to the feedback line of the closed loop control scheme (Fig. 1). Two modes of data sampling in analyzing feedback output from the BLDC motor have been tested: (1) equal angular separation and (2) equal time intervals. In case (1), the data are collected via equal intervals $\Delta\theta$ of the rotor's sequential angular position θ_i, i = 1, 2, 3, …, i.e., keeping $\Delta\theta$ = const. In case (2), the data collection time points t_i are separated by equal sampling time intervals Δt = const, thus ensuring constant sampling rate $r_s = 1/\Delta t$.

In the equal angular separation mode, the motor supplied the sequence of operating voltages which according to the state model would lead to the desired values of the state variables. In the equal time intervals sampling mode, the sequence of operating voltages is affected by the estimates of the outcoming states of BLDC motor conducted by the Kalman filter (KF).

The Logic Controller in Fig. 1 aims to reach speed ω_{ref}. In our task, the need is to explore motor's behavior within the full range of available speeds under a given set of system's parameters. To achieve that, the value of ω_{ref} is to be chosen above the upper bound ω^{upper} of the observable speeds, otherwise it is scaled up and the experiment is repeated to ensure $\omega_{ref} > \omega^{upper}$.

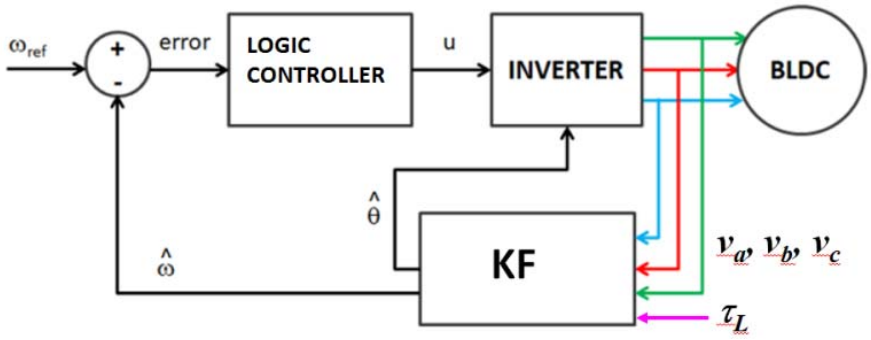

Fig. 1 Schematic of the employed closed loop control system of BLDC motor with Kalman filter in the feedback loop. Kalman filter's inputs are operating voltages v_a, v_b and v_c for the motor's phases A, B and C, while outputs are estimated values of angular speed ω and rotor's angular position θ

A. BLDC Motor Model

The BLDC state space model is derived (see [10]) based on established electromagnetic interactions in the motor windings. It is to be used for the more complex speed estimation methods and will assume that the motor has a trapezoidal shaped back EMF. The motor is assumed to have three identical phases of which one can model only one phase and apply it to the rest of the phases. By using this consideration, the first equation for the phase becomes:

$$u_a = Ri_a + (L - M)\frac{di_a}{dt} + \xi_a + u_n, \quad (1)$$

u_a is the phase voltage, R is the phase resistance, i_a is the phase current, L is the phase inductance, M is the mutual inductance, ξ_a is the phase back EMF voltage, u_n is the neutral node voltage.

The back EMF is assumed to be trapezoidal, therefore the commutation scheme becomes such that only two phases are active at the same time. Then the neutral voltage can be presented as in the following:

$$u_n = \frac{1}{3}[(u_a + u_b + u_c) - (\xi_a + \xi_b + \xi_c)] \quad (2)$$

Combining the above equations brings about the following:

$$\frac{di_a}{dt} = \frac{u_{ab} - u_{ca}}{3(L-M)} - \frac{R}{(L-M)}i_a + \frac{\xi_b + \xi_c - 2\xi_a}{3(L-M)} \quad (3)$$

The back EMF can be expressed as a function of angular velocity rather than that of voltage. Now all three phases need to be accounted for, so that proper commutation maintains 120-degrees shifts between the phases. In this case the back EMF components become:

$$\xi_a = K_\xi \omega f(\theta) \quad (4)$$

$$\xi_b = K_\xi \omega f(\theta - \tfrac{2\pi}{3}) \quad (5)$$

$$\xi_c = K_\xi \omega f(\theta + \tfrac{2\pi}{3}) \quad (6)$$

with function $f(\theta)$ being defined as:

$$f(\theta) = \begin{cases} \frac{6}{\pi}\cdot\theta, 0 \le \theta < \frac{\pi}{6} \\ 1, \frac{\pi}{6} \le \theta < \frac{5\pi}{6} \\ -\frac{6}{\pi}\cdot(\theta - \pi), \frac{5\pi}{6} \le \theta < \frac{7\pi}{6} \\ -1, \frac{7\pi}{6} \le \theta < \frac{11\pi}{6} \\ \frac{6}{\pi}\cdot(\theta - 2\pi), \frac{11\pi}{6} \le \theta < 2\pi \end{cases} \quad (7)$$

The function $f(\theta)$ has the trapezoidal shape for a 360-degrees electrical cycle. The phase current equations thus can be expressed as:

$$\frac{di_a}{dt} = \frac{u_{ab} - u_{ca}}{3(L-M)} - \frac{R}{(L-M)}i_a + \frac{K_\xi \omega\left[f\left(\theta - \frac{2\pi}{3}\right) + f\left(\theta + \frac{2\pi}{3}\right) - 2f(\theta)\right]}{3(L-M)} \quad (8)$$

$$\frac{di_b}{dt} = \frac{u_{bc} - u_{ab}}{3(L-M)} - \frac{R}{(L-M)}i_b + \frac{K_\xi \omega\left[f(\theta) + f\left(\theta + \frac{2\pi}{3}\right) - 2f\left(\theta - \frac{2\pi}{3}\right)\right]}{3(L-M)} \quad (9)$$

$$\frac{di_c}{dt} = \frac{u_{ca} - u_{bc}}{3(L-M)} - \frac{R}{(L-M)}i_c + \frac{K_\xi \omega\left[f(\theta) + f\left(\theta - \frac{2\pi}{3}\right) - 2f\left(\theta + \frac{2\pi}{3}\right)\right]}{3(L-M)} \quad (10)$$

The equation for angular velocity can be obtained from expression for electromagnetic torque in combination with the conversion of electrical degrees into mechanical ones and expression for mechanical motion torque, resulting in:

$$\frac{d\omega}{dt} = \frac{p^2 K_\xi}{J}\left[f(\theta)i_a + f\left(\theta - \frac{2\pi}{3}\right)i_b + f\left(\theta + \frac{2\pi}{3}\right)i_c\right] - \frac{p\tau_L}{2J} - \frac{B\omega}{J} \quad (11)$$

Matrices of the state space equations from the above become:

$$\boldsymbol{A} = \begin{bmatrix} -\frac{R}{(L-M)} & 0 & 0 & F_{14} & 0 \\ 0 & -\frac{R}{(L-M)} & 0 & F_{24} & 0 \\ 0 & 0 & -\frac{R}{(L-M)} & F_{34} & 0 \\ \frac{p^2 K_\xi}{J} f(\theta) & \frac{p^2 K_\xi}{J} f(\theta - \frac{2\pi}{3}) & \frac{p^2 K_\xi}{J} f(\theta + \frac{2\pi}{3}) & -\frac{B}{J} & 0 \\ 0 & 0 & 0 & 1 & 0 \end{bmatrix} \quad (12)$$

$$\boldsymbol{B} = \begin{bmatrix} \frac{1}{3(L-M)} & 0 & 0 & 0 \\ 0 & \frac{1}{3(L-M)} & 0 & 0 \\ 0 & 0 & \frac{1}{3(L-M)} & 0 \\ 0 & 0 & 0 & -\frac{p}{2J} \\ 0 & 0 & 0 & 0 \end{bmatrix} \quad (13)$$

$$\vec{x} = \begin{bmatrix} i_a \\ i_b \\ i_c \\ \omega \\ \theta \end{bmatrix} \quad (14)$$

$$\vec{u} = \begin{bmatrix} u_{ab} - u_{ca} \\ u_{bc} - u_{ab} \\ u_{ca} - u_{bc} \\ \tau_L \end{bmatrix} \quad (15)$$

$$F_{14} = \frac{K_\xi \omega \left[f\left(\theta - \frac{2\pi}{3}\right) + f\left(\theta + \frac{2\pi}{3}\right) - 2f(\theta) \right]}{3(L-M)} \quad (16)$$

$$F_{24} = \frac{K_\xi \omega \left[f(\theta) + f\left(\theta + \frac{2\pi}{3}\right) - 2f\left(\theta - \frac{2\pi}{3}\right) \right]}{3(L-M)} \quad (17)$$

$$F_{34} = \frac{K_\xi \omega \left[f(\theta) + f\left(\theta - \frac{2\pi}{3}\right) - 2f\left(\theta + \frac{2\pi}{3}\right) \right]}{3(L-M)} \quad (18)$$

Here R is the phase resistance; L is the phase inductance; M is the mutual inductance; p is the number of poles; K_ξ is the back EMF constant; J is the rotor inertia; $f(\theta)$ is the normalized trapezoidal function; B is the motor viscous damping friction; i_a, i_b, i_c are the phase currents; u_{ab} - u_{ca} is the applied phase a voltage; u_{bc} - u_{ab} is the applied phase b voltage; u_{ca} - u_{bc} is the applied phase c voltage; τ_L is the applied mechanical torque load; θ is the electrical angle; ω is the electrical angular velocity.

B. Kalman Filter Estimator for BLDC Motor

The Kalman filter is an estimator with statistical properties to estimate an output based on a mathematical model. The estimator considers the errors produced by process, estimation and measurement noise and under assumption of all noise to be Gaussian distributed it estimates an output. The discrete Kalman estimator can be in two different states, the prediction step where the estimator tries to predict the current system state, and the correction step where the so called Kalman gain is computed and the system state is estimated. The Kalman estimator can be described with equations:

Prediction step:

$$\hat{x}_k^- = \boldsymbol{A}\hat{x}_{k-1}^- + \boldsymbol{B}\vec{u}_k \quad (19)$$

$$\boldsymbol{P}_k^- = \boldsymbol{A}\boldsymbol{P}_{k-1}\boldsymbol{A}^T + \boldsymbol{Q} \quad (20)$$

Correction step:

$$\boldsymbol{K}_k = \boldsymbol{P}_k^-\boldsymbol{C}^T(\boldsymbol{C}\boldsymbol{P}_k^-\boldsymbol{C}^T + \boldsymbol{R})^{-1} \quad (21)$$

$$\hat{x}_k = \hat{x}_k^- + \boldsymbol{K}_k(\vec{z}_k - \boldsymbol{C}\hat{x}_k^-) \quad (22)$$

$$\boldsymbol{P}_k = (\boldsymbol{I} - \boldsymbol{K}_k\boldsymbol{C})\boldsymbol{P}_k^- \quad (23)$$

where $\boldsymbol{A}$, $\boldsymbol{B}$ and $\boldsymbol{C}$ are the matrices of the state space equations; $\hat{x}_k^-$ is the estimated state (prior); $\hat{x}_{k-1}^-$ is the previous estimated state; $\hat{x}_k$ is the estimated state output; $\vec{u}_k$ is the input vector; $\boldsymbol{P}_k$ is the state error covariance matrix; $\boldsymbol{Q}$ is the process noise error covariance matrix; $\boldsymbol{R}$ is the measurement error covariance matrix; $\boldsymbol{K}_k$ is the Kalman gain; $\boldsymbol{I}$ is the identity matrix; z_k is the measurement vector. Herewith the Kalman estimator is only used with a position-sensorless scheme; therefore, the current is the only sensor measurements. As the variance of the current is assumed to be 0.1A, the measurement noise error matrix $\boldsymbol{R}$ becomes:

$$\boldsymbol{R} = \begin{bmatrix} 0.1 & 0 & 0 \\ 0 & 0.1 & 0 \\ 0 & 0 & 0.1 \end{bmatrix} \quad (24)$$

The chosen variance values are: 0.02A for the currents, 50 rpm for the angular velocity and π/36 (5°) for the position. Hence, the $\boldsymbol{Q}$ matrix assumes the form:

$$\boldsymbol{Q} = \begin{bmatrix} 0.02 & 0 & 0 & 0 & 0 \\ 0 & 0.02 & 0 & 0 & 0 \\ 0 & 0 & 0.02 & 0 & 0 \\ 0 & 0 & 0 & 50 & 0 \\ 0 & 0 & 0 & 0 & \frac{\pi}{36} \end{bmatrix} \quad (25)$$

In the MATLAB implementation of the Kalman filter for BLDC motor, the following initial set of parameters had been employed in the program (we call it herewith as "base set") and initialized as following (in MATLAB notations):

```
T = 0.000020; % seconds
L = 0.02; M = 0.01; % Henry
R = 1; % initialize resistance R;
Kemf = 1; % back-EMF coefficient
tauL = 1; % is the applied mechanical torque load
p = 4; %% number of poles
Bd = 1; % Bd is the motor viscous damping friction;
J = 1; % is the rotor inertia
```

The non-diagonal elements of the 4-th column of the matrix A have been represented by the 2-D array F1234, which was defined (in MATLAB notations) as:

```
F1234 = zeros(3,N);
for n = 1:N
 F1234(1,n) = [Kemf/(3*(L-M))]*(ftetaM(n)+ftetaP(n)-
2*fteta(n));
 F1234(2,n) = [Kemf/(3*(L-M))]*(fteta(n)+ftetaP(n)-
2*ftetaM(n));
 F1234(3,n) = [Kemf/(3*(L-M))]*(fteta(n)+ftetaM(n)-
2*ftetaP(n));
end
```

IV. Simulation Results

Simulated is closed loop control scheme of Fig. 1 with Kalman filter in the feedback line to provide position sensorless drive of BLDC motor. In the model two distinguished separate data sampling modes are verified by Kalman filter in analyzing feedback output from the BLDC

motor: (1) equal angular separation increments mode and (2) equal time intervals mode. In the first case, the data are sampled by Kalman filter via estimated equal intervals $\Delta\theta$ of rotor's angular position θ_i, thus keeping $\Delta\theta$ = const and varying sampling rate as the rotor's speed varies. In the second case, the Kalman filter maintains the separation between data sampling time points t_i to be equal, so that sampling time intervals Δt = const. The result of modeling and simulation implementation in terms of the effects of the systems parameters on the performance of the sensorless control scheme is presented below.

A. Equal Angular Increments in Driving of BLDC Motor

For the equal angular increments drive simulation of BLDC motor, the following relations between voltage variables have been used in the program (MATLAB notations):

```
for n = 1:N %1200 steps
 uAB(n) = uA(n)-uB(n);
 uAC(n) = uA(n)-uC(n);
 uBC(n) = uB(n)-uC(n);
 Uabca(n) = uAB(n)+uAC(n);
 Ubcab(n) = uBC(n)-uAB(n);
 Ucabc(n) = -uAC(n)-uBC(n);
 uk(1,n) = Uabca(n);
 uk(2,n) = Ubcab(n);
 uk(3,n) = Ucabc(n);
end
```

Here, N = 1200 is the number of time-steps for a single rotation cycle of the rotor. Synchronization of the driving voltages for the motor's phases, measured with respect to the ground, is shown in Fig. 2.

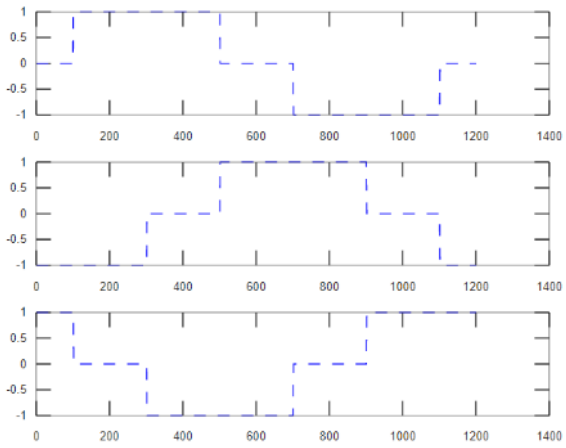

Fig. 2 Operating voltages for the motor's phases A, B and C measured with respect to the ground (parameters used in the program are: uAG, uBG, uCG). Voltages are represented in relative units (proportional to K_V = 100 V scaling up factor). Horizontal scale is in relative step units, scaled by 20 μsec/step

Four tests have been conducted for the equal angular increments driving mode: (1) starting of BLDC motor from zero position; (2) rotor acceleration stage which follows the start of BLDC motor; (3) saturation of acceleration and (4) reaching of the steady state rotation. The results of the above tests are as follows:

Test case #1 is the starting of BLDC motor from initial position, i.e. when orientation angle and initial speed are both equal zero, while rotation cycle number M = 1. The dynamic of the evolution of the state variables during the first driving cycle (i.e., test #1) is presented in Fig. 3. It is seen that proper commutation of the winding's currents results in rotor acceleration, which is higher in the first half of the very first cycle of rotation.

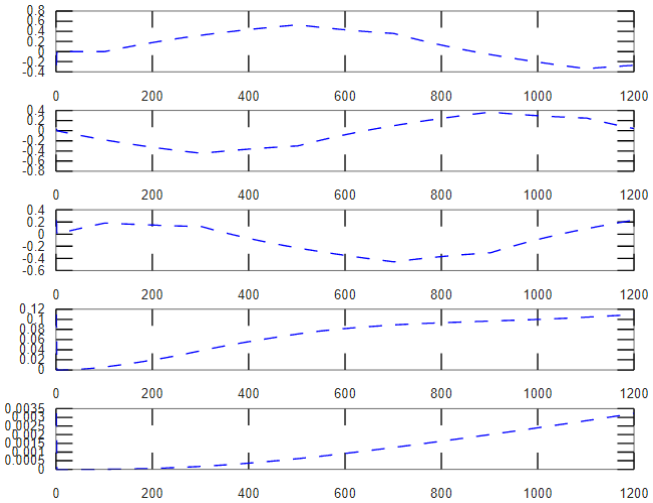

Fig. 3 Test case #1. Starting of BLDC motor from zero position (zero orientation angle, zero initial speed, cycle number M = 1). Shown sequentially are state variables: three phase currents, angular speed and electrical angle. Vertical scales are in relative units (proportional to amps for phase currents, rad/sec for angular speed and rad for angular position). Horizontal scale is in relative step units, scaled by 20 μsec/step

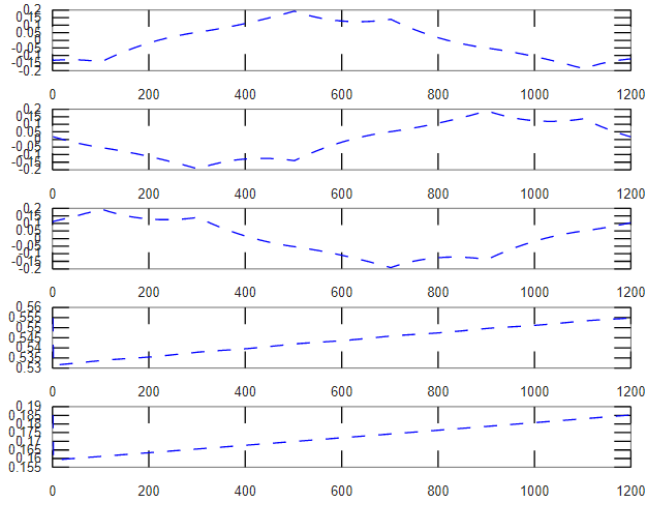

Fig. 4 Test case #2. Rotor acceleration stage after the start of BLDC (verification at 11-th rotation cycle, M = 11). Shown sequentially are state variables: three phase currents, angular speed and electrical angle. Vertical scales are in relative units (proportional to amps for phase currents, rad/sec for angular speed and rad for angular position). Horizontal scale is in relative step units, scaled by 20 μsec/step

The rotor's acceleration is progressively increasing with the cycles to follow, as test #2 confirms in Fig. 4 for the 11-th rotation cycle, i.e., for M = 11.

The growth of acceleration eventually saturates leading to the occurrence of the torque ripples after about 100 rotations, as test #3 demonstrates in Fig. 5 for the 111-th rotation cycle, i.e., for M = 111.

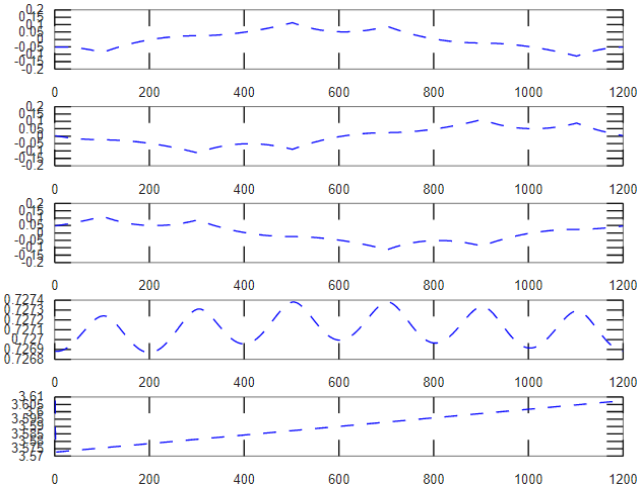

Fig. 5 Test case #3. Saturation of acceleration and reaching of the steady state rotation after 100 rotations are done (verification at 111-th rotation cycle, M = 111). State variables are 3 phase currents, angular speed and electrical angle. Vertical scales are in relative units (proportional to amps for phase currents, rad/sec for angular speed and rad for angular position). Horizontal scale is in relative step units, scaled by 20 μsec/step

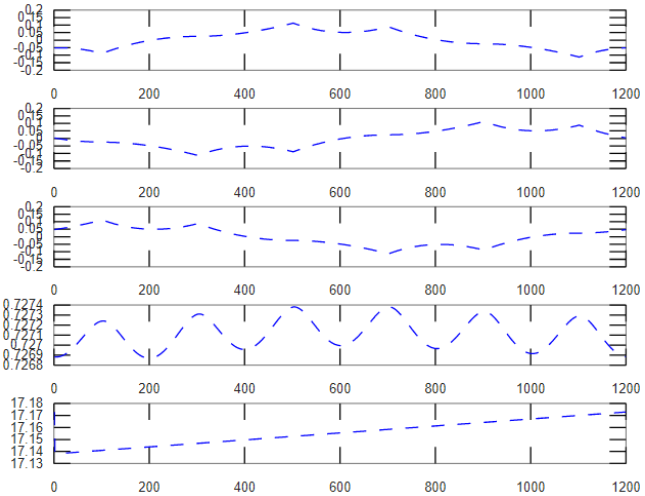

Fig. 6 Test case #4. Steady state rotation after 500 rotations (verification at 500-th rotation cycle, M = 500). Shown sequentially are state variables: three phase currents, angular speed and electrical angle. Vertical scales are in relative units (proportional to amps for phase currents, rad/sec for angular speed and rad for angular position). Horizontal scale is in relative step units, it is to be scaled by 20 μsec/step

The trend continues reaching steady state rotation after about 500 rotations, which is verified by test #4 in Fig. 6 for the 500-th rotation cycle, i.e., for M = 500.

After rotation speed reaches a certain level, the values of generated back EMF become big enough to sustain closed loop sensorless control.

B. Equal Time Increments in Driving of BLDC Motor

An equal time increments drive of BLDC motor is achieved herewith by engaging KF estimator in the feedback line with the constant sampling rate to estimate the commutation instances. The entry level of the initial angular speed for closed loop sensorless control is about 1000 rotations/min. From the entry level of angular speed, the sensorless control continues evolution to the upper speed level. The tests for an equal time increments drive therefore will be conducted on sequence of consecutive rotations presented here as "frames" with dynamic changes of the state variables. The performance of the closed loop control of BLDC motor with KF in an equal time increments drive is shown in Fig. 7. Seen is the occurrence of instability ripples featuring two modulation frequencies – lower frequency is equal to that of the rotation, and the higher frequency is six times higher (in 3 phases and 2 poles case).

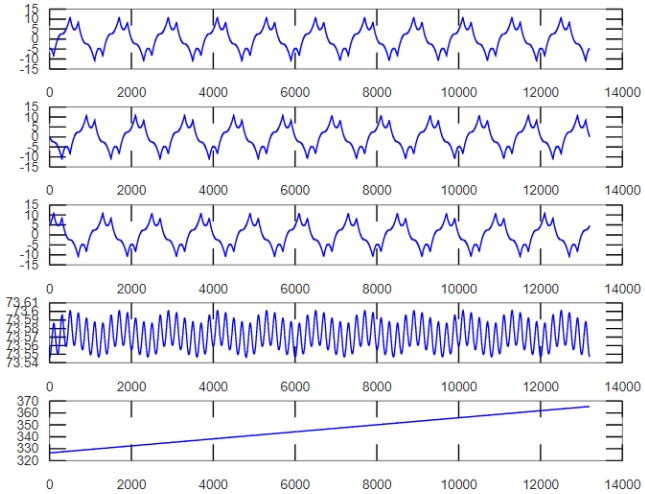

Fig. 7 Closed loop control of BLDC motor by KF with an equal time increments drive. Shown are 10 consecutive frames with starting frame being #101 and ending frame #111

We attribute the origin of such ripples to the inaccuracy in timing of switching the commutations, which in turn is due to discrete nature of sampling and limitation of matching continuous process with discrete steps. Such inaccuracy lays the ground for instability which manifests itself in the induced ripples. The increase of induction twice (to L = 0.04 and M = 0.02 Henry) reduces amplitude of the instability ripples proportionally, as it is shown in Fig. 8.

Changing discretization time in KF estimator also affects instability ripples. Specifically, reducing discretization time T from 20 microseconds (as in Fig. 8) to 15 microseconds facilitates reduction of instability ripples as it is seen in Fig. 9.

Balancing of the torque load with amplification coefficient K_V for input voltages to the motor is shown in Fig. 10. The

coefficient converts input voltages from the one given in Fig. 2 to actual input voltages by K_V as a scaling factor. In Fig. 10 the load changes at a time t = 1 sec from 0 to 20 microN. Appropriate change of K_V to balance to rotation speed changes from K_V = 100 to K_V = 125.

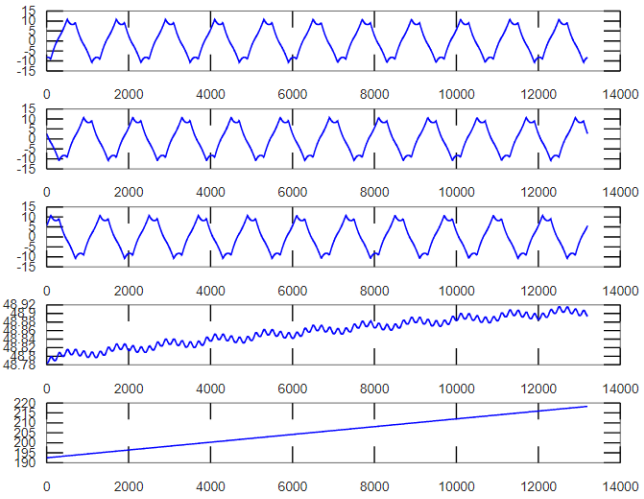

Fig. 8 Reduction of instability ripples via motor's induction increase (twice as compared to that of Fig. 7 and reaching L = 0.04 and M = 0.02 Henry)

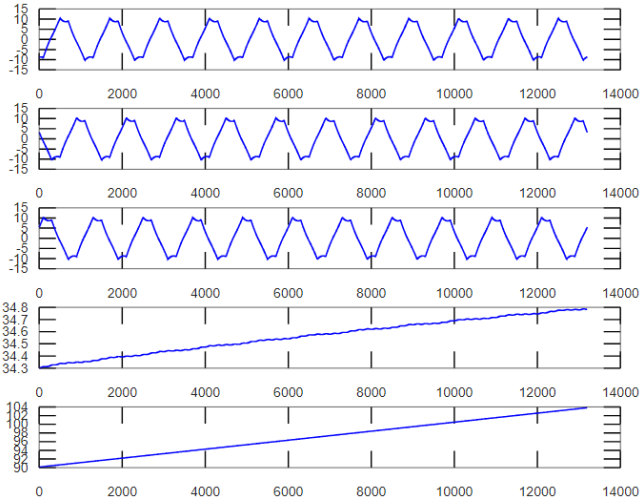

Fig. 9 Further reduction of torque ripples via reduction of Kalman filter discretization time Δt = T down to 15 μsec. Other parameters are the same as in Fig. 7

V. Conclusion

Implemented is the closed loop control model of BLDC motor with the Kalman filter in control feedback line for position sensorless drive. Demonstrated are variations in sensorless control performance of BLDC motor from system's parameters involved, including those of Kalman filter, BLDC motor and operating circuits. For the mode of equal angular increments verified are the following cases of sensorless control: (1) initial acceleration of the BLDC's rotor from starting position; (2) speeding up of the rotor to reach the prescribed rotation speed; (3) saturation of the acceleration; (4) reaching of the steady state rotation and (5) occurrence of the commutation induced instability ripples. For equal angular increments, drive mode control with Kalman filter estimator in the feedback line demonstrated is: (1) suppression of the commutation induced instability ripples via sampling rate increase of employed Kalman filter above critical threshold value; (2) increase of the computational cost of the above torque ripples suppression for the motors with smaller induction values of its windings; (3) torque load balancing via adjustment of the input voltage scaling up coefficient in the logic of the controller.

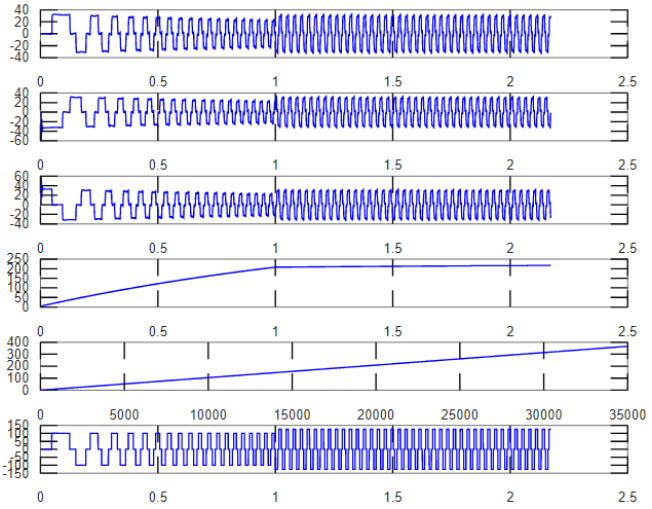

Fig. 10 Balancing of the torque load change at a time t = 1 sec from 0 to 20 microN with the proportional change of scaling factor for input voltages from K_V = 100 to K_V = 125. Upper 5 plots are dependences of state variables from running time t (in seconds). Last plot adds dynamics of K_V to the picture

References

[1] A practical approach to Kalman Filter and how to implement it. url: http://blog.tkjelectronics.dk/2012/09/a-practical-approach-to-kalman-filter-and-how-to-implement-it/.

[2] Muntaka Musa Bari Usman Abubakar Abdulaziz Bello Ibrahim Muhammad Kilishi. Comparative Review of PMSM and BLDCM Based on Direct Torque Control Method". In: International Journal of Scientific and Technology Research 3.2277-8616 (2014), pp. 195-199.

[3] About Commutation and Current Control Methods for Brushless Motors (Retrieved 2016-10-22). url: http://www.drivetechinc.com/articles/curbldc3.pdf.

[4] Mahmoud Kassas Adeel Sabir. A Novel and Simple Hybrid Fuzzy/PI Controller for Brushless DC Motor Drives". In: AUTOMATIKA 4.56 (2015), pp. 424{435. doi: http://dx.doi.org/10.7305/automatika.2016-01-1053.

[5] Analog Devices, Low cost Complete 12-bit RDC (Retrieved 2016-10-17). url: http://www.analog.com/media/en/technical-documentation/data-sheets/AD2S90.pdf.

[6] Brushless DC Motors Part 1: Construction and Operating Principles (Retrieved_2016-09-08). url: http://www.edn.com/design/sensors/4406682/Brushless-DC-Motors---Part-I--Construction-and-Operating-Principles.

[7] Tomita, M., Senjyu, T., Doki, S., et al. (1998) New sensorless control for brushless DC motors using disturbance observers and adaptive velocity estimations. IEEE Transactions on Industrial Electronics, 45(2), 274–282.

[8] Terzic, B., Jadric, M. (2001) Design and implementation of the extended Kalman filter for the speed and rotor position estimation of brushless DC

motor. IEEE Transactions on Industrial Electronics, 48(6), 1065–1073.
[9] Shi, T. N., Lu, N., Zhang, Q., et al. (2008) Brushless DC motor sliding mode control with Kalman filter. IEEE International Conference on Industrial Technology, 4, 1–6.
[10] Mattias Johansson, "Evaluation of Sensor Solutions & Motor Speed Control Methods for BLDCM /PMSM in Aerospace Applications". - Master Thesis, Space Engineering, Specialization Spacecraft & Instrumentation. Lulea University of Technology, 2017, Sweden.